J Nanopart Res (2022) 24: 43
https://doi.org/10.1007/s11051-022-05422-6

BRIEF COMMUNICATION

Photocatalytic activity of graphene oxide quantum dots in an effluent from a South African wastewater treatment plant

C. S. Tshangana · A. A. Muleja · B. B. Mamba

Received: 20 July 2020 / Accepted: 24 January 2022 / Published online: 15 February 2022

Abstract Graphene oxide quantum dots (GOQDs) were used as photocatalysts under visible light for the discoloration of synthetic and real wastewater spiked with organic azo dye. The GOQDs were synthesized using a one-pot method involving the pyrolysis of citric acid. The characterization of the synthesized GOQDs using XPS, FTIR, XRD, Raman, UV-Vis, FEEM, Zetasizer and TEM confirmed the successful synthesis of the nanosized materials. The results of the photocatalytic experiments showed efficient degradation of the dye, which amounted to 60% and 98% over a period of 180 min for the synthetic water and spiked real wastewater, respectively. The pseudo-first-order model was found to be a better fit for both the synthetic and spiked real wastewater samples. The coefficient of correlation (R^2) of 0.991 and 0.996 was obtained for the synthetic and real wastewaters, respectively. The rate of discoloration decreased with increasing concentration of the dyes. The data demonstrated that an increase in the reaction rate constant resulted in faster dye discoloration and higher catalytic activity and yielded shorter half-lives. The degradation of dye was attributed to a combination of photocatalytic mechanism and photosensitization degradation emanating from the self-degradation of photoexcited dyes. The reactive oxygen radicals and holes played a role in the degradation of the dye molecules. Additionally, the photolytic contribution was minor, while the photocatalytic activity of GOQDs was the major to the degradation process. The results showed that GOQDs can be used in the treatment of wastewater effluent for the detoxification and discoloration of the harmful dye.

Keywords Detoxification · Photosensitization · Nanosized · Azo dye · Photodegradation · Environmental effects

This article is part of the topical collection: Nanotechnology Convergence in Africa

Guest Editors: Mamadou Diallo, Abdessattar Abdelkefi, and Bhekie Mamba

C. S. Tshangana · A. A. Muleja (✉) · B. B. Mamba
Institute for Nanotechnology and Water Sustainability (iNanoWS), College of Science, Engineering and Technology, University of South Africa, Johannesburg 1709, Florida, South Africa
e-mail: mulejaa@unisa.ac.za

Introduction

Advanced oxidative processes (AOPs) are increasingly being applied in environmental remediation (Putri et al. 2016; Syam Babu et al. 2019; Gandhi et al. 2016; Sharma and Philip 2016). The conversion of solar energy into chemical energy through AOP provides an excellent platform to address both the environmental problems and energy issues. Among the known AOPs, photocatalysis has been widely used in wastewater treatment applications. As a result, AOPs have garnered a lot of attention over the last 10 years with more than 16,000 scientific papers relating to photocatalysis being published (Scopus) (Rueda-Marquez et al.

2020). The majority of the work documented on the use of AOPs in wastewater treatment focussed on the degradation and reduction of the toxicity of organic dyes using model solutions (Tsai and Tseng 2020; Topkaya et al. 2014; Wang et al. 2020; Tshangana et al. 2020a; Muleja and Mamba 2018). Studies on the photodegradation of organic dyes in model solutions have demonstrated the efficiency of these photocatalysts. The effect of numerous parameters such as the pH value, the actual composition of the water, ion concentration, competing ions and the presence of organic and inorganic substances are rarely taken into account. As a result, the performance of the photocatalyst will differ significantly when tested in real water versus when tested in model solutions in the laboratory.

Avisar et al. (Avisar et al. 2013) investigated the impact of the water matrix in the removal of carbamazepine using different water matrices (groundwater, surface water, distilled water, demineralized water, secondary effluent and tertiary effluent). Results from Avisar et al. study (Avisar et al. 2013) demonstrated that the use of distilled or demineralized water was not ideal matrices to evaluate the photocatalytic efficiency in the removal of organic pollutants. The results obtained when using either distilled or demineralized water matrices were not reflective of the photodegradation efficiency of the photocatalysts, and in most instances, the results were found to be rather too optimistic and not painting an accurate picture of what would occur in real water. These studies further demonstrated that even adding humic acid to deionized water did not accurately simulate real-world water conditions.

The aforementioned reasons paved a way for more researchers to investigate the detoxification of real industrial and municipal wastewater. Some of the types of water evaluated include real pharmaceutical industry wastewater (Talwara et al. 2018), municipal wastewater effluent spiked with ibuprofen (Jalloulia et al. 2018), sewage wastewater spiked with malathion, fenitrothion (Vela et al. 2018a), effluent from urban wastewater treatment plant spiked with pharmaceutically active compounds (PhACs) (He et al. 2016), textile wastewater (Lima et al. 2015), textile effluent from jeans industrial laundry (Souza et al. 2016) and sewage wastewater effluent spiked with endocrine disruptors (Vela et al. 2018b) to name a few. The photocatalysts used in the above-mentioned studies were either TiO_2 or ZnO, both of which have been widely used in photocatalytic applications. In this work, however, graphene oxide quantum dots (GOQDs) were deployed as photocatalysts. Unlike TiO_2 or ZnO, GOQDs have high electron mobility as well as a bandgap that can be tailored for different purposes by varying the shape, size and edge chemistry (Pan et al. 2010). GOQDs are also able to provide a direct path for the transport of photo-generated charge carriers, which in turn result in increased lifetimes of the electron–hole pairs and have demonstrated upconversion behaviour. In addition, GOQDs have a large surface area, large diameter and fine surface grafting through the π–π conjugated network or surface groups (Shen et al. 2012). All these features make GOQDs suitable for photocatalytic applications.

The use of GOQDs in the discoloration and detoxification of wastewater spiked with BB dye is addressed in this study. The study's main goals were to (a) synthesize and fully characterize GOQDs, (b) determine the photocatalytic degradation and discoloration of wastewater spiked with BB dye under various conditions (different light intensities and water matrices) and (c) elucidate the photodegradation mechanism of the BB dye using GOQDs.

Experimental details

Preparation of graphene oxide quantum dots (GOQDs)

Graphene oxide quantum dots were prepared using a combination of two previously reported approaches as described in our previous paper (Tshangana et al. 2020b). The fabrication of GOQDs involved heating 5 g of citric acid (Sigma-Aldrich, South Africa) in a round-bottom flask for 30 min at 240 ºC. The white crystalline powder of the citric acid was left to melt into a colourless light-yellow liquid, which eventually turned into dark orange. The melted citric acid was dissolved in 100 mL of 10 mg/mL solution of NaOH. The NaOH was prepared by dissolving NaOH pellets (Sigma-Aldrich, South Africa) in Milli-Q ultrapure water (Millipore Corp., Bedford, MA, USA). Column chromatographic separation of the resultant solution using silica gel (Sigma-Aldrich, South Africa) and 0.01 M HCl (Sigma-Aldrich, South Africa) as the eluent gave an aqueous solution of GOQDs. Figure 1 shows the schematic preparation of GOQDs.

The GOQDs were characterized using several techniques. Fourier transform infrared spectroscopy (FTIR) analysis of the GOQDs was performed on a

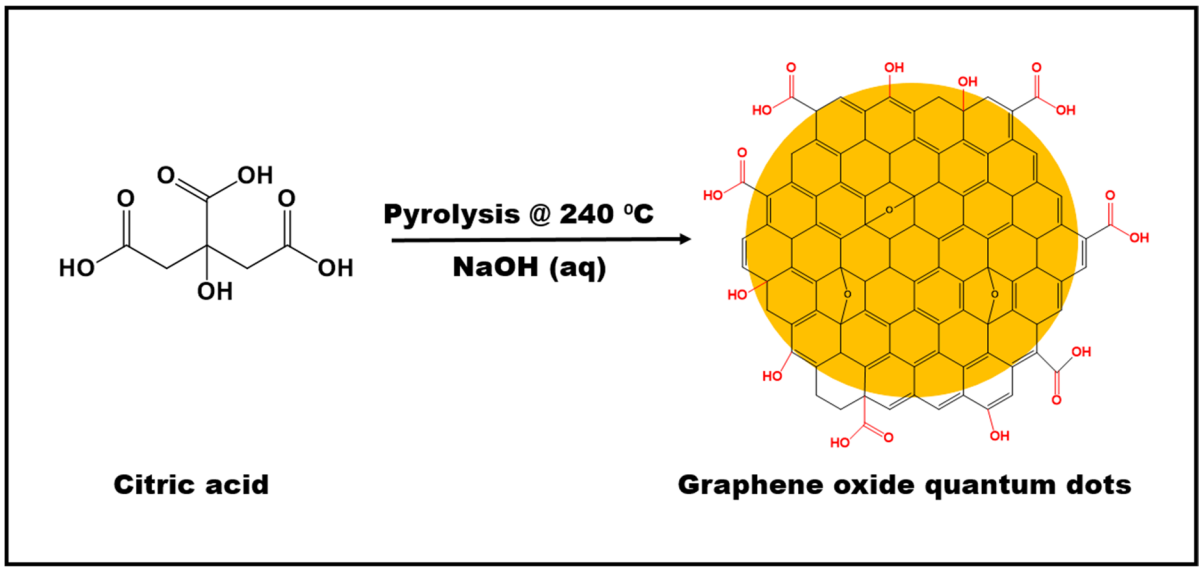

Figure 1 Synthesis of GOQDs by pyrolysis of citric acid

Bruker Alpha IR (100 FTIR). Raman analysis was carried out using a confocal Raman spectrometer (XploRA™ Plus HORIBA Scientific, France SAS) equipped with 514 nm laser that is used to collect spectral data. Ground state electronic absorption spectra were recorded using UV-Vis-2550 spectrophotometer (Shimadzu 1800). The emission spectra were obtained using fluorescence excitation emission matrix (FEEM) fluorescence (Aqualog, HORIBA, Jobin Yvon) in the wavelength range 200–830 nm. The excitation was set at 2 nm, and the emission interval value was 3.28 nm. The surface charge of the GOQDs was measured using Malvern Zetasizer nanoseries, Nano-ZS90. X-ray photoelectron spectroscopy (XPS) analysis was carried out using AXIS Ultra equipped with Al (monochromatic) anode and a charge neutralizer. A transmission electron microscopy (TEM) micrograph was obtained from a Zeiss Libra 120 TEM operating at 80 kV. X-ray diffraction (XRD) patterns were collected using a Bruker D8 Discover equipped with a Lynx Eye detector, using Cu-Ka radiation (= 1.5405 A°, nickel filter). The data were collected in the range from 20 = 10° to 100°, scanning at 1° min^{-1}, filter time constant of 2.5 s per step and a slit width of 6.0 mm. Prior to analysis, the samples were placed on a silicon wafer slide. The X-ray diffraction data were processed using Eva (evaluation curve fitting) software. Using XRD data, the sizes of GOQDs were determined using the Debye–Scherrer equation (Eq. 1) (Sapra and Sarma 2005):

$$d = \frac{0.9\lambda}{B\cos\theta} \quad (1)$$

where d is the mean diameter of a quantum dot in nanometers (nm), λ the wavelength of the X-ray source (1.5405 Å), β the full width at half maximum of the diffraction peak and θ the angular position of the peak.

Sampling site and sample collection

The wastewater effluent sample was obtained from a South African WWTP. Wastewater at this specific WWTP goes through different stages including a primary clarifier, an aeration tank, a secondary clarifier and finally a disinfection unit where bacteria are removed. Keeping this in mind, for the purpose of this study, the sampling point selected was before the primary clarifier. A multi-parameter meter (YSI Professional Plus) was used to measure the pH and electrical conductivity (EC). Orion TM AQUAfast AQ3010 Turbidity Meter was used to analyse the turbidity, while the total organic carbon (TOC) was measured using a Teledyne Tekmar TOC Fusion. The

water quality parameters of the collected wastewater sample are summarized in Table 1.

The sampling approach used to collect the wastewater was as follows: glass sampling bottles (1 litre) were washed with a laboratory detergent and rinsed thoroughly with tap water. Thereafter, the sampling bottles were soaked at room temperature and for 24 h in aqua regia (1:3 vol by volume (v/v) ratio of HNO_3:HCl) (Sigma-Aldrich, South Africa). To reduce any possible contamination caused by trapped air, the sample bottles were filled to the brim with wastewater with no headspace. Upon arrival at the laboratory, the wastewater samples were stored at 4 °C in a refrigerator.

Photocatalytic activity evaluation

The photocatalytic performance of the GOQDs was evaluated by measuring the rate of degradation of a model organic pollutant and colourant, Brilliant Black (BB) dye, in synthetic water and real wastewater samples. Organic dyes are some of the major chemical pollutants found in industrial and other effluents that find their way into a water treatment plant and eventually into environmental water bodies. For this reason, the BB dye was specifically selected to mimic the real effluent from the wastewater treatment plant where real wastewater was sampled.

Four sets of experiments were conducted, namely, (a) the first experiment involved the use of BB dye (Sigma-Aldrich, South Africa) as a model organic pollutant. To this end, 1 mg of GOQDs was added to the BB dye solution (10 ppm, 50 mL); (b) in the second experiment, wastewater sample collected from a treatment plant was spiked with 10 ppm of the BB dye, and 1 mg of GOQDs was added to 50 mL solution (15 mL BB dye solution + 35 mL wastewater); (c) for the control experiments, 1 mg of GOQDs was added to wastewater (50 mL) without spiking with BB dye; and (d) similar experiments were carried out as described above at varying pH values.

Table 1 Water quality parameters of the collected wastewater

Properties	Values
pH	6.9 ± 0.25
Turbidity (NTU)	110 ± 3.26
TOC (mg $C.L^{-1}$)	22.30 ± 0.032
Electrical conductivity (μS cm^{-1})	743 ± 5.31
DO	10.9 ± 0.054

The effect of changing light intensities on the photodegradation rate was performed by using (a) white light-emitting diodes (LED) strips and (b) a solar simulator. The configuration of the LED reactor was as follows: the LED lights (20 mW) (the irradiation was measured using a Digital Lux Meter and was found to be approximately 80 mW cm^{-2}) were mounted around the inner walls of a customized stainless steel rectangular reactor. The set-up was completed with a magnetic stirrer and beaker. The experimental set-up was covered with an aluminium foil to shield it from light. The solar simulator used (HAL-320 supplied by ASAHI SPECTRA (Japan)) was equipped with a 300-W compact xenon lamp and an Air Mass 1.5 Global filter which produced irradiation of approximately 100 mW cm^{-2}.

In both experimental set-ups prior to conducting the photocatalytic experiments, the solutions (mixtures of GOQDs and synthetic water; GOQDs and spiked wastewater) were stirred in the dark for 30 min, after which the lights were switched on. Aliquots of the solutions (3 mL) were withdrawn using a disposable syringe at 30-min intervals over a period of 180 min. The aliquots were filtered using a 0.45-μm PVDF filter paper (Sigma-Aldrich, South Africa). Variations in the concentrations of the BB dye were monitored by measuring the absorbance of the filtrate using a Perkin Elmer Lambda 650s UV-Vis spectrophotometer. The photodegradation efficiency was calculated using the following (Eq. 2):

$$\text{Degradationrate}(\%) = \left(1 - C_t/C_i\right)\text{x}100 \quad (2)$$

where C_i and C_t represent the initial concentration of BB dye at times i and t, respectively.

Kinetic studies

The reaction kinetics of BB dye degradation was studied, the results were fitted to a pseudo-first-order model, and a plot based on the calculated $\text{In}(C_t/C_i)$ versus the irradiation time t was obtained from the linear form of Eq. 3:

$$\ln(C_t/C_i) = -kt \quad (3)$$

where k refers to the pseudo-first-order rate constant, C_t is the concentration of BB dye at a specific time after irradiation, and C_i is the initial concentration of BB dye. The reaction rate was obtained using Eq. 4:

$$\text{rate} = k(C) \quad (4)$$

where k refers to the pseudo-first-order rate constant and C is concentration of the dyes. The half-life time ($t_{1/2}$) of the photocatalytic reactions were determined using Eq. 5:

$$t_{\frac{1}{2}} = 0.693/k \quad (5)$$

Radical scavenging experiments

To investigate reactive species generated in the photodegradation process and to elucidate the photodegradation mechanism, radical scavenging experiments were carried out. The same experimental procedures as described above (*Photocatalytic activity evaluation* section) were carried out with the introduction of different radical scavengers at the beginning of the experiments. The radical scavengers used in the experiments had the same concentration of 60 mM. Silver nitrate, ethylenediaminetetraacetic acid disodium (EDTA-2Na), methanol and benzoquinone were used as scavengers for electrons (e^-), holes (h^+), hydroxyl radicals (•OH) and superoxide ($\bullet O_2$), respectively (Shafaee et al. 2018). Thereafter, the aliquots were filtered using a 0.45 µm PVDF filter and analysed using a Perkin Elmer Lambda 650s UV-Vis spectrophotometer.

Photocatalyst reusability experiments

Reusability experiments were carried out to determine the stability and recyclability of the GOQDs photocatalyst. This is key parameter for practical applications; the reused GOQDs (from the first cycle) were separated, recovered by centrifugation and dried in an oven and tested under the same experimental conditions as described in the *Photocatalytic activity evaluation* section for an addition three additional cycles.

Results and discussion

Photocatalytic activity of graphene oxide quantum dots

The photocatalytic performance of the fabricated GOQDs was studied by evaluating the degradation of the BB pollutant dye in synthetic water and wastewater samples. The respective time-dependent absorption spectra of degradation of the BB dye are presented in Figure 2. An incubation period of 30 min in the dark was carried out prior to irradiating with light; this was done to allow the adsorption–desorption process between the dye molecules and the catalyst to reach equilibrium. After 180 min of irradiation, significant degradation of the dye was observed for the dye in the synthetic (60% degradation) and wastewater (98% degradation) samples. In the control experiment (without the dye), there was a negligible reduction in degradation percentage of 11%. The huge difference in the degradation percentage of the two samples is attributed to the pH; the BB dye in the synthetic water sample (pH value of 4.1) contains non-dissociated carboxylic acids and epoxide groups (Loh et al. 2010). In solution, the negatively charged surface of the GOQDs (−23.47 mV) is the majority species, and the repulsive forces dominate resulting in the reduced of the adsorption of the dye. For the wastewater sample spiked with the BB dye (pH 7.0),

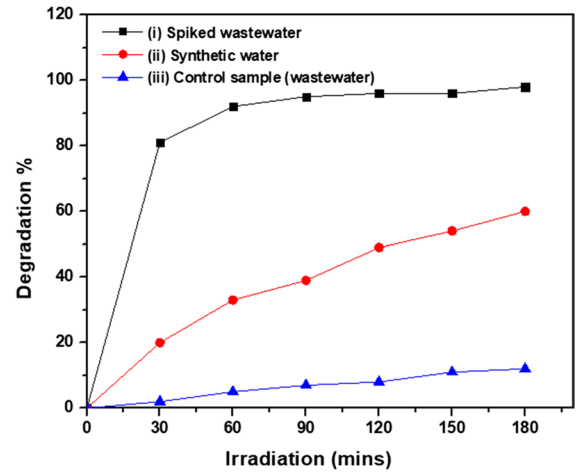

Figure 2 Influence of different water matrices on the photocatalytic activity of GOQDs in the degradation of BB dye in **i** spiked wastewater, **ii** synthetic water and **iii** the control experiments without BB dye

the carboxylic acids and phenolic OH are ionized, and the negatively charged surface of the GOQDs attracts the positively charged BB dye cations (Konkena and Vasudeva 2012). Elsewhere, Ge et al. (Ge et al. 2016) demonstrated that GOQDs were able to degrade up to 100% rhodamine B (RhB) after 12 min of irradiation time. This finding shows that when compared to traditional catalysts, GOQDs work better under visible light irradiation.

Figure 3 shows the photographical images of the discoloration process after 180 min of irradiation of the BB dye in both samples (i.e. BB dye in synthetic water and wastewater spiked with BB dye) when GOQDs are used as a photocatalyst. In aqueous solution, the deep purple-coloured BB dye (10 ppm) changed to a very light purple colour when 1 mg of GOQDs as added at room temperature and under irradiation conditions (Figure 3a). The discoloration of the dye contaminated water indicates that chromophores present in the dye molecules are destroyed in the presence of GOQDs. The destruction of the conjugated chromophore results from the breaking down of both the azo and aromatic groups, which are responsible for bonding the dye molecules (Ge et al. 2016; Xu et al. 2020). According to Xu et al. (Xu et al. 2020), the activity of the photocatalyst is enhanced when composites of oxidized nanoporous g-C_3N_4 (PCNO) are decorated with graphene oxide quantum dots (ox-GOQDs). The features contributing to the enhancement of the photocatalyst include ameliorated light-harvesting ability, higher charge transfer efficiency, enhanced photooxidation capacity and increased amounts of reactive species due to the upconversion properties and strong electron capturing ability. Moreover, GOQDs are known to possess an excellent electron transfer ability, which is key in enhancing photocatalytic efficiency (Xiong et al. 2020). In addition, the high conductivity and strong electron capturing ability of ox-GOQDs allow easier access to electrons and the electron diffusion process becomes much more effective, ultimately leading to an improvement in the charge transfer efficiency of the photocatalysts (Zhang et al. 2018). The discoloration can also be ascribed to low pH conditions because the H^+ ions are able to compete with the dye species resulting in a decreased in colour removal efficiency compared to when the wastewater sample were used (Figure 3b).

Kinetic studies

The degradation kinetics was studied using different light intensities to better understand the degradation behaviour of the BB dye molecules as depicted in Figure 4. Under different light intensities, the photodegradation of the BB dye followed the pseudo-first-order kinetics.

A reduced photocatalytic efficiency was expected in the wastewater sample owing to the complex composition of the wastewater. The obtained results proved otherwise; similar observations were made by Matamoros et al. (Matamoros et al. 2008). The authors studied the effect of different water matrices (freshwater and river water) on the photodegradation of carbamazepine. The results obtained from the study showed an enhanced photodegradation of carbamazepine in river water. To explain this phenomenon, the authors ascribed the improved photodegradation efficiency of the carbamazepine to the high dissolved oxygen content (DOC) in the river water.

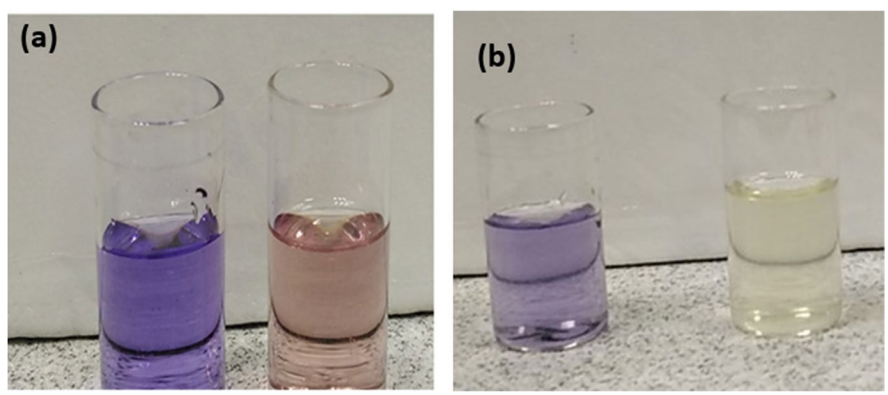

Figure 3 Colour change of **a** synthetic water and **b** wastewater spiked with BB dye before and after addition of GOQDs under visible light irradiation for 180 min

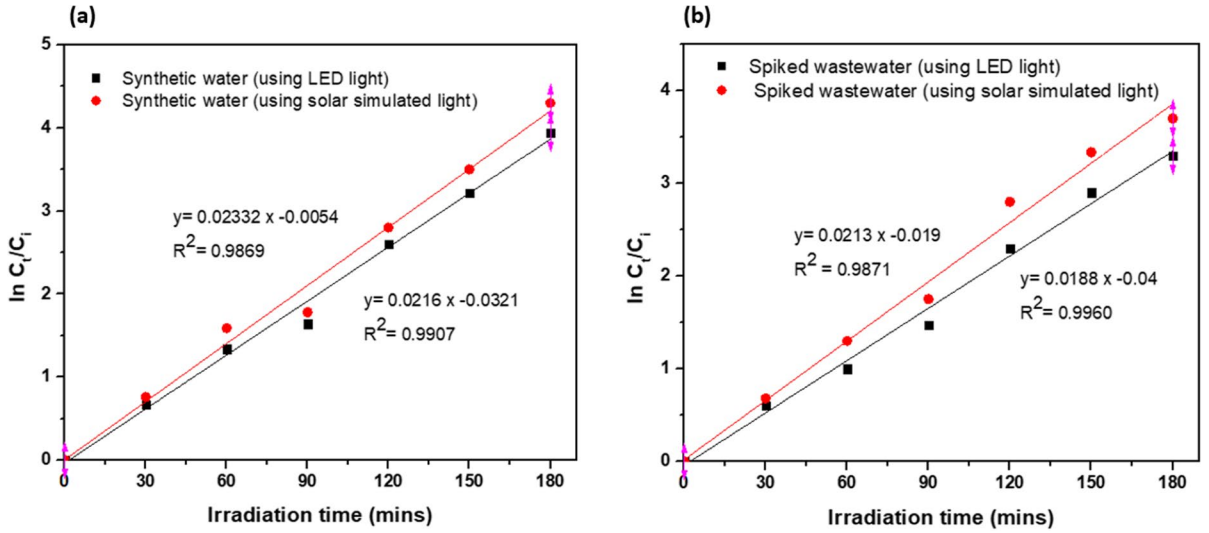

Figure 4 Pseudo-first-order kinetics of BB dye degradation using 1 mg of GOQDs in 10 ppm under LED light and simulated solar light for (**a**) synthetic water and (**b**) spiked wastewater samples

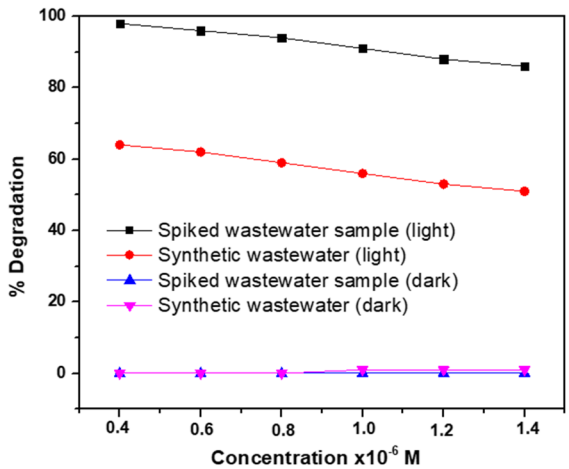

Figure 5 The effect of initial BB dye concentrations on the degradation efficiencies of the GOQDs under light and dark conditions

Similarly, in this study, we postulate the presence of natural organic matter (NOM). and the high DOC in the wastewater sample enhanced the BB dye degradation via indirect slow photodegradation during the photocatalytic processes. Hence, explaining why, the wastewater sample had a higher photodegradation efficiency than the synthetic water sample.

The degradation efficiency of the GOQDs when the initial concentration of the BB dye was varied is depicted in Figure 5. Figure 5 shows a similar trend whereby the concentration of the BB dye in both samples results in a decrease in the degradation percentage. These results demonstrate that the degradation percentage is strongly dependent on the concentration of BB dye molecules in the solution. When the concentration of the BB dye molecules in solution was increased, more BB dye molecules were adsorbed on the surface of the GOQDs. An increase in the concentration of the BB dye means that the active sites of the GOQDs become blocked, thus reducing the efficiency of the photocatalyst. The increase in the concentration of the BB dye also leads to a decrease in the number of photons reaching the surface of the GOQDs. Similar findings were reported by Rajabi et al. (Rajabi and Farsi 2015).

Kinetic data (see Table 2) was obtained by plotting the different concentrations of the BB dye against the irradiation time. Both the synthetic water and spiked wastewater samples were found to possess higher reaction rates (k) at lower BB concentrations, and as the concentrations increased the reaction rates (k), values decreased. The decrease in the reaction rates (k) is expected since an increase in BB dye concentration results in photons entering the solution being intercepted, thus reducing photodegradation rates of BB dye at higher concentrations (Rajabi and Farsi 2015). At lower BB concentrations, the opposite is true; a higher number of protons are absorbed.

Table 2 Rate constant (k), half-life ($t_{1/2}$), maximum dye decolourization and R^2 values and of various initial concentrations of BB dye in synthetic water and spiked wastewater in the presence of GOQDs

BB dye concentration ($\times 10^{-6}$ M)	k ($\times 10^{-3}$ min^{-1})		Half-life (min)		Maximum discoloration (%)		R^2 values	
	Synthetic water	Spiked wastewater	Synthetic water	Spiked wastewater	Synthetic water	Spiked wastewater	Synthetic water	Spiked wastewater
0.40	0.0393	0.0427	17.63	14.84	64	98	0.8974	0.9314
0.60	0.0314	0.0418	22.07	16.58	62	95	0.9051	0.9089
0.80	0.0290	0.0371	23.09	18.68	59	93	0.9126	0.9866
1.00	0.0274	0.0315	25.29	22.00	56	91	0.8908	0.9329
1.20	0.0248	0.0309	27.94	22.43	53	88	0.9733	0.9779
1.40	0.0210	0.0261	33.00	26.55	50	85	0.8901	0.9398

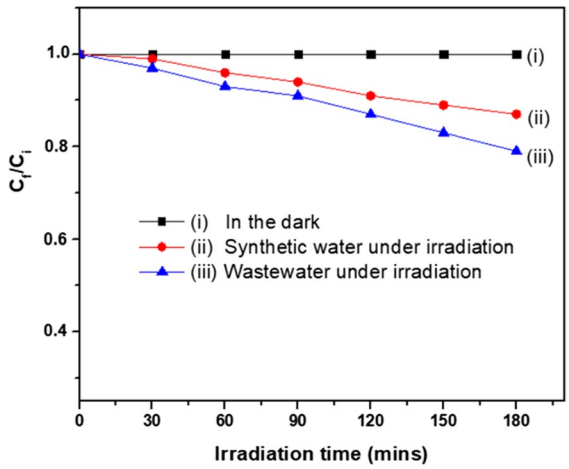

Figure 6 Photolysis of BB dye in the absence of GOQDs and under the LED light irradiation

In addition, a specific trend was noted whereby an increase in reaction rate constant resulted in faster dye decolourization, higher catalytic activity and shorter half-lives.

To understand the mechanism of photodegradation further and to determine whether the degradation of the BB dye was as a result of the photocatalyst (GOQDs) or light (self-photolysis), experiments were conducted in the absence of GOQDs. Figure 6 shows that zero degradation of the dye was observed for the sample that was kept in the dark without irradiation. At the same time, 16% and 26% of the BB dye were degraded in the synthetic water and the spiked wastewater sample, respectively, thus providing evidence that self-photolysis forms part of the degradation mechanism. The data indicate that, without the self-photolysis reaction, photocatalytic activity accounts for approximately 76% of the degradation of BB dye in the real wastewater sample. Previously, researchers (Shao et al. 2011; Xiang et al. 2013) have attributed self-photolysis to the self-degradation of photoexcited dyes. However, as observed in Figure 2, the degradation of the BB dye is significantly enhanced by the addition of GOQDs. It can be concluded that, while photosensitization degradation is one of the pathways in which degradation of the BB dye is achieved, the photodegradation mechanism in this research work is the dominant pathway. As can be seen from Figure 6, photocatalysis is the dominant mechanistic pathway responsible for the degradation of BB dye molecules. The data presented in Figure 6 rules out adsorption as the main mechanistic pathway followed in the degradation of BB dye in both the synthetic and real wastewater samples. It is recommended that additional studies be conducted at the exit of the WWTP to determine the efficiency of this method.

Identifying radicals responsible for the photodegradation of BB dye

Radical scavenging experiments were carried out to determine the contribution and influence of each radical responsible for the photodegradation of BB dye. Excess methanol, EDTA-2Na, p-benzoquinone and silver nitrate were used as scavengers for •OH, h^+, $\bullet O_2^-$ and e^-, respectively. Figure 7 shows that h^+ (13%) and e^- (7%) contributed the least to the degradation of BB dye. Methanol on the other hand inhibited 82% of the •OH radicals, making the •OH the

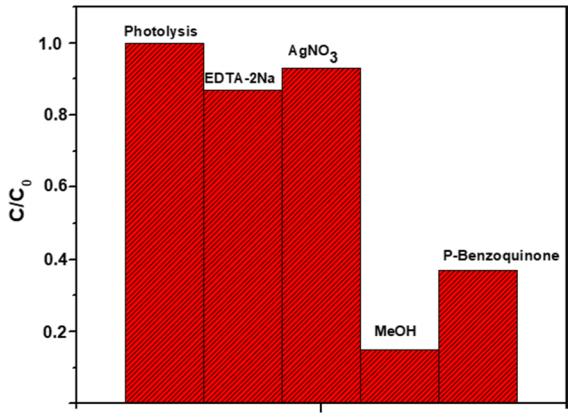

Figure 7 Quenching experiments using EDTA-2Na, $AgNO_3$, methanol and p-benzoquinone for comparative purpose experiments in the dark are also included

greatest contributor, while p-benzoquinone inhibited 63% of the $\bullet O_2^-$.

Proposed mechanism

Based on data from the quenching experiments on Figure 7, a photocatalytic degradation pathway was proposed (Figure 8a). When both GOQDs and the BB dye absorb sufficient light, the electron (e^-) in the valence band of the GOQDs gets excited, leaving a hole (h^+), and the migration of the electrons to the conduction band results in the generation of the e^-/h^+ pair (Eqs. 6–10). The e^-/h^+ pair can be transferred to the surfaces and interact with H_2O molecules, producing peroxide (O_2^-) and hydroxyl radical ($^\bullet$OH) species, respectively, which are very reactive in the degradation of organic pollutant (Rahimi et al. 2018):

$$GOQDs \rightarrow GOQDs\left(e^-_{CB} + h^+_{VB}\right) \tag{6}$$

$$GOQDs\left(e^-_{CB}\right) + \left(O_2\right)_{ads} \rightarrow GOQDs + \left(O_2^{\bullet -}\right)_{ads} \tag{7}$$

$$\left(O_2^{\bullet -}\right)_{ads} + H^+ \rightarrow HO_2^\bullet \tag{8}$$

$$2HO_2^\bullet \rightarrow H_2O_2 + O_2 \tag{9}$$

$$H_2O_2 + e^- \rightarrow OH^- + OH^\bullet \tag{10}$$

Additionally, the valence band holes can directly oxidize the organic pollutant (BB dye) adsorbed on the surface of photocatalyst (GOQDs) which can act as a barrier against the recombination of e^-/h^+ pair in order to remain reactive for longer times (Rahimi et al. 2018). Alternatively, the valence band holes can also indirectly mineralize the BB dye via hydroxyl radicals ($\bullet$OH) generated

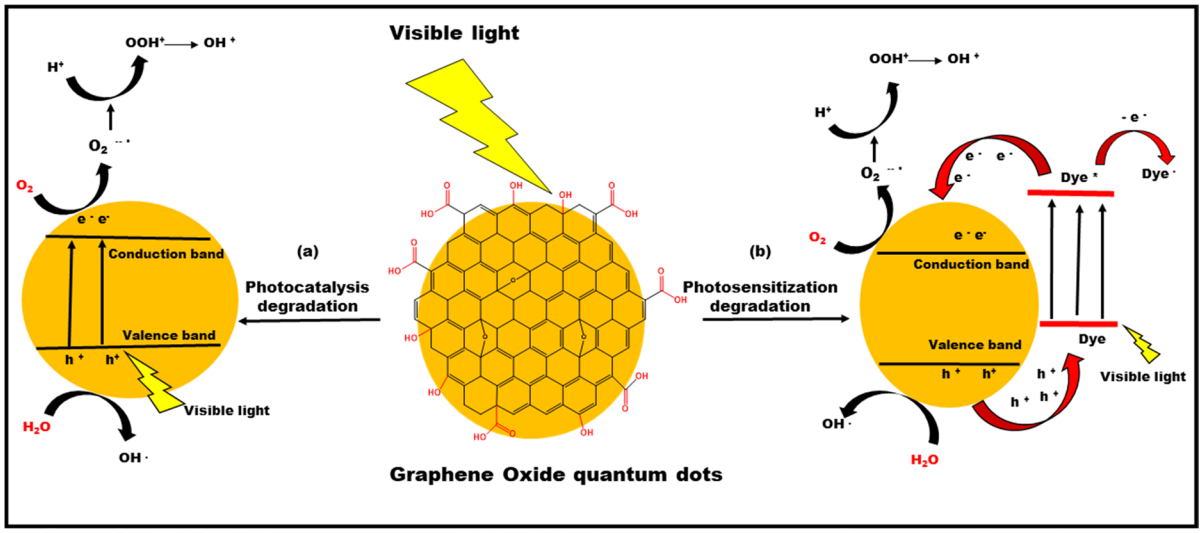

Figure 8 Proposed mechanisms of degradation of BB dye which can occur via (**a**) photocatalysis degradation or (**b**) photosensitization degradation in synthetic water and real wastewater spiked using 1 mg of GOQDs

when holes and water (H_2O) molecules react or are chemisorbed (OH^-) (Eqs. 11–13) (Wang et al. 2011):

$$GOQDs\left(h^{+}{}_{VB}\right) + \left(H_2O\right)_{ads} \rightarrow GOQDs + \left(HO^{\bullet}\right)_{ads} + \left(H^{+}\right)_{ads} \quad (11)$$

$$\mathrm{GOQDs}\left(\mathrm{h}^{+}{}_{\mathrm{VB}}\right) + \left(\mathrm{HO}^{-}\right)_{\mathrm{ads}} \rightarrow \mathrm{GOQDS} + \left(\mathrm{HO}^{\bullet}\right)_{\mathrm{ads}} \quad (12)$$

$$\mathrm{GOQDs}\left(\mathrm{h}^{+}{}_{\mathrm{VB}}\right) + \mathrm{Dye}_{\mathrm{ads}} \rightarrow \mathrm{GOQDs} + \left(\mathrm{Dye}^{\bullet+}\right)_{\mathrm{ads}} \quad (13)$$

For the photosensitization degradative pathway (Figure 8b), the large surface area of GOQDs (Shen et al. 2012) allows the efficient adsorption of BB dye molecules. When irradiated, the electrons in the ground state of the dye gets excited; some of the excited electrons can be transferred to the CB of the GOQDs. This allows the photoinduced active species (e.g. $\bullet O_2^-$, •OOH, •OH) to oxidize or degrade the organic pollutants absorbed on the surface of the GOQDs as shown in Eqs. 14–16:

$$Dye + hU(vis) \rightarrow Dye^{*} \quad (14)$$

$$Dye^{*} + GOQDs \rightarrow Dye^{\bullet+} + GOQDs\left(e^{-}{}_{CB}\right) \quad (15)$$

$$GOQDs\left(h^{+}{}_{VB,}{}^{\bullet}OH,{}^{\bullet}OOHorO_2{}^{\bullet-}\right) + Dye \rightarrow CO_2 + H_2O + smallby - products \quad (16)$$

The proposed mechanism is based on the mechanism that has been reported for homogenous photocatalysts (Kim et al. 2014; Roushani et al. 2015). Although the proposed mechanism is not yet fully understood, we postulate that the degradation of the BB dye in both waters involves the irradiation of the dyes molecules and it proceeds via both photocatalytic and photosensitization degradation (see Figure 8 and Eqs. 6–16).

Photocatalyst reusability experiments

Reusability experiments were conducted to determine the stability and recyclability of the GOQD photocatalyst which is a key parameter for practical applications. The reused GOQDs (from the first cycle) were separated, recovered by centrifugation and dried in an oven and tested under the same experimental conditions as described in the *Photocatalytic activity evaluation* section for an addition of two additional cycles. The photodegradation performances of the GOQDs in both wastewater and synthetic water after 4 cycles are shown in Figure 9. As the number of cycles increases, it was noted that the degradation rates of the GOQDs decreased gradually from 98.0% of the first cycle to 85.9% after the fourth cycle.

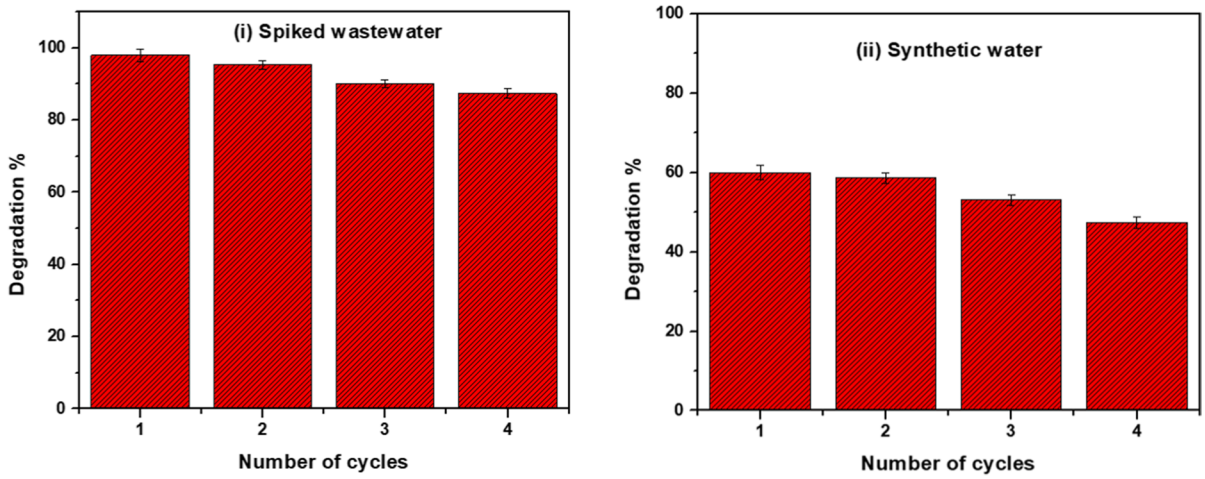

Figure 9 Reusability experiments of the GOQDs in **i** spiked wastewater and **ii** synthetic water

This trend is expected because as the GOQDs are reused, the number of active sites inevitably gets reduced. It is encouraging to see that even after 4 cycles, the GOQDs were still able to remove more than 85% of the dye. Even in the synthetic water samples, the photodegradation reduced from 60 to 47%. The interesting reusability performances of the GOQDs suggest GOQDs are stable and can therefore be applied in water treatment applications.

Characterization of the prepared GOQDs

The structural composition of the GOQDs was probed using XPS; for the full scan (presented in Figure 10a), the signals for C1s, O1s and the Na auger peak were observed at 286.3, 531 and 495 eV, respectively. The emergence of the Na auger peak at 495 eV was ascribed to the NaOH used during the synthesis procedure. For the XPS wide scan (Figure 10b), the C1s peak of the GOQDs was deconvoluted into three carbon species that are centred at 285.1, 287.5 and 288.4 eV; these chemically distinct carbons are attributed to the sp^3 carbon (C-C, C-O), the sp^2 carbon (C=C) and the oxidized carbon (C=O), respectively.

The FTIR spectrum of GOQDs (Figure 11a) is characterized by a broadened peak appearing in the range 3100–3600 cm^{-1}, which is attributed to the O-H stretching vibrations. A stretching vibration of C-H is evidenced by the peak appearing at 2962 cm^{-1}. The stretching vibration of the C-O appeared in the range of 1273 cm^{-1}. The vibration of C-O suggests that the GOQDs contain some incompletely carbonized citric acid (Zhu et al. 2011). The peaks at 1710 cm^{-1} and 1621 cm^{-1} are characteristic of the stretching vibrations of the C=O of carboxylic and/or carbonyl moiety. The FTIR spectrum presented in this work is similar to the one reported in the literature (Tang et al. 2012; Štengl et al. 2013; Manna et al. 2018).

The XRD pattern of the GOQDs is shown in Figure 11b. A prominent peak is observed at $2\theta = 27$, which is ascribed to (002) Bragg's reflection and an interlaying spacing of 0.36 nm (Zhang et al. 2013; Tetsuka et al. 2012). The prominent peak indicates that the carbonization of citric acid produced GOQDs that have a more compact interlayer spacing than the original graphene. In agreement with previously reported findings (Hashemzadeh et al. 2016; Puvvada et al. 2012), the synthesized GOQDs are structurally similar to graphite. The average crystallite sizes of the GOQDs were determined using the Debye–Scherrer equation (Eq. 1). The sizes were found to be 3.1 nm, and the broadness of the XRD peak at 27° also shows that the crystallite sizes are small.

The Raman spectrum of the GOQDs was obtained using Raman spectrometer employing a 514 nm laser as the excitation source. The two prominent peaks (Figure 12a) at 1362 cm^{-1} and 1611 cm^{-1} are characteristic of the GOQDs peaks (Chhabra et al. 2018) and resemble the disordered "D" band and a graphic (crystalline) "G" band, respectively. The "D" band arises from the disorder present on the surface of GOQDs. The surface states (i.e. sp^3 C–C, sp^3 C–O

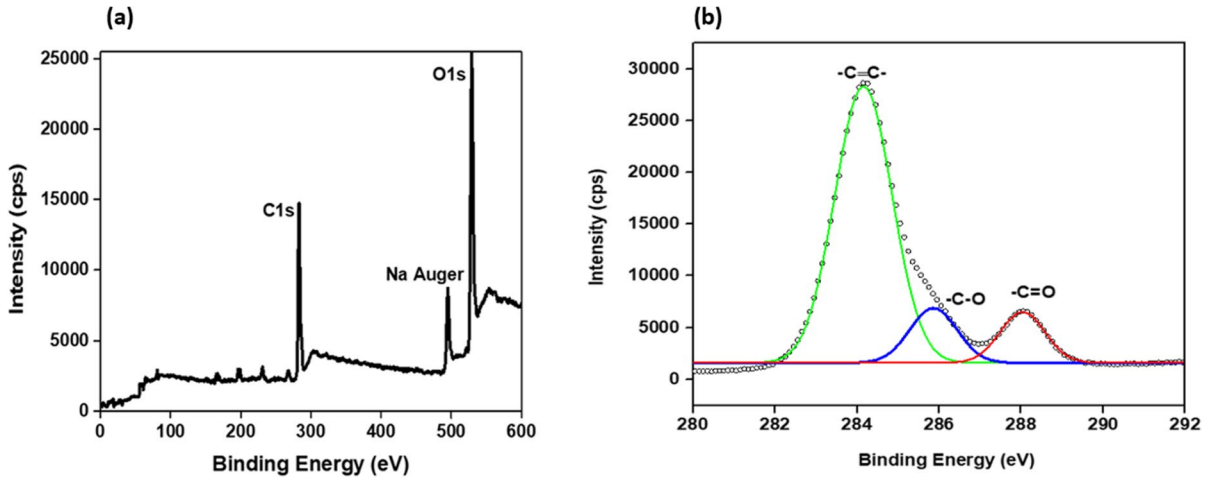

Figure 10 **a** XPS wide scan survey and **b** high-resolution XPS spectra of the synthesized GOQDs

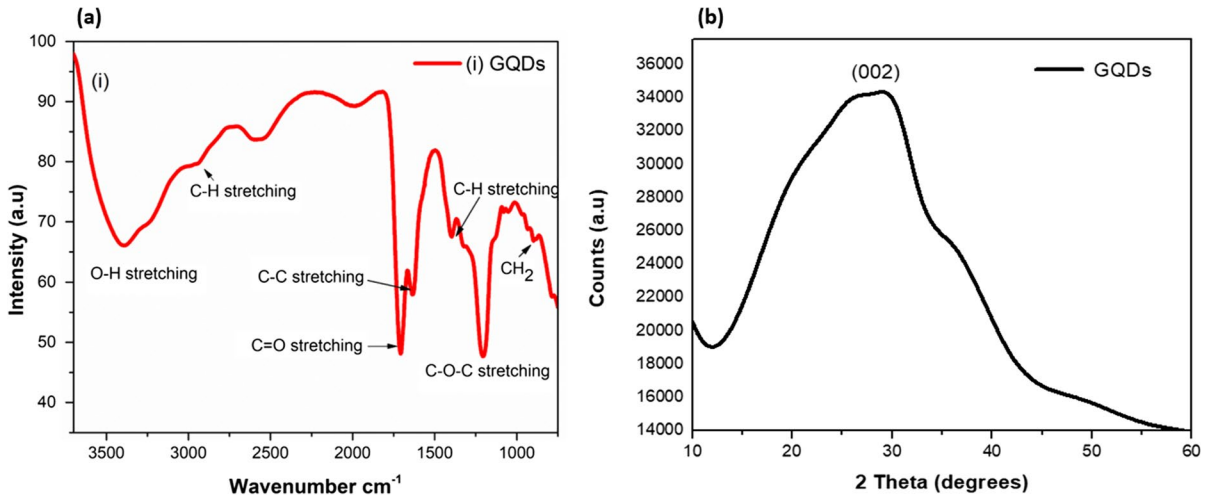

Figure 11 Chemical structure of GOQDs: **a** FTIR spectrum and **b** XRD pattern

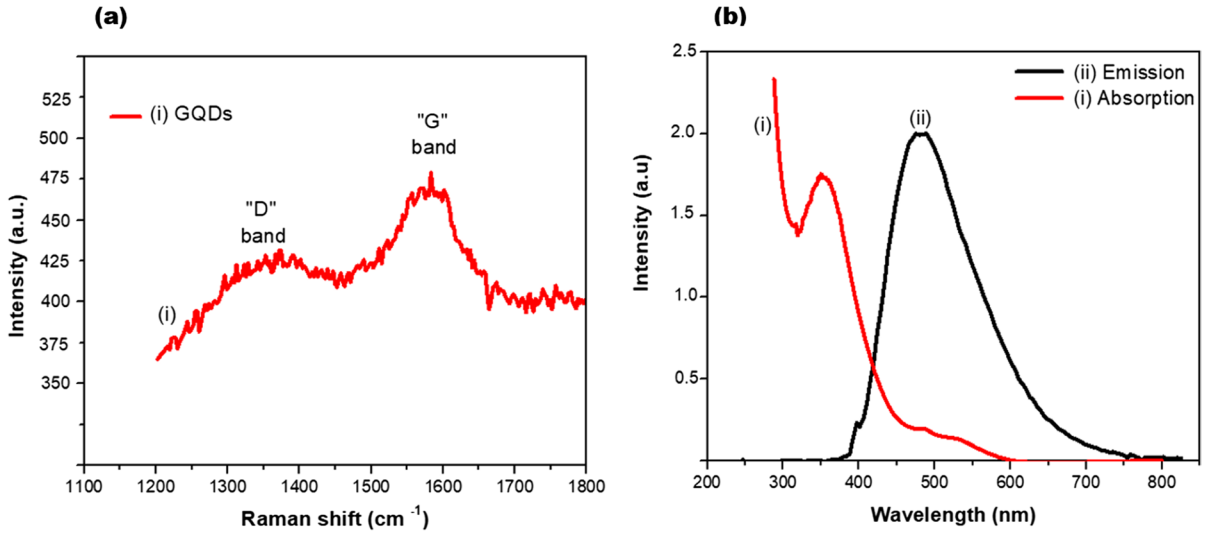

Figure 12 **a** Raman spectrum of GOQDs and **b** absorption and emission spectra of GOQDs

and sp^2 C=O) result in the broadening of "D" band. The "G" band on the other hand is characteristic of carbon materials possessing the sp^2 C=C bonds. The "G" band is ascribed to stretching of sp^2 C=C bond and arises from the vibration of E_{2g}st phonon at Γ-point (Kudin et al. 2008; Sobon et al. 2012). The extent of sp^2/sp^3 hybridization of the carbon atoms is expressed using the ratio of the intensity of the "D" and G bands (I_D/I_G ratio). An I_D/I_G value of 0.845 was obtained, which confirms the highly crystallized structures of the single layered-GOQDs (Zhang et al. 2012).

Figure 12b shows the absorption and emission spectra of the GOQDs. An intense absorption peak in the UV region at 351 nm is ascribed to the π → π* transition (i.e. radiative recombination of electron hole pair) of sp^2 C=C bonds. A shoulder peak in the visible region at 480 nm is due to the n → π* transition (i.e. localized levels in band gap) of surface functional groups (Qu et al. 2013). The GOQDs display

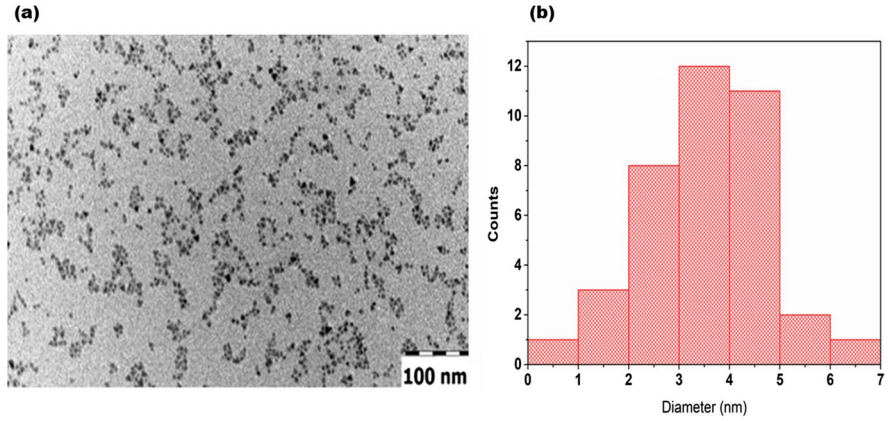

Figure 13 **a** Transmission electron microscopy (TEM) image of GOQDs and **b** the corresponding particle size distribution histogram

fluorescence properties as indicated by the emission peak at 480 nm at an optimal excitation wavelength of 390 nm. Our findings corroborate previously reported studies on GOQDs (Kumar et al. 2010).

The morphology of the GOQDs was analysed with TEM. The TEM micrograph of the GOQDs (Figure 13a) shows that the GOQDs were of various shapes, mostly spherical, monodispersed and not aggregated. The average particle size was found to be 4.3 nm. The average particle sizes based on TEM were obtained by plotting the particle size distribution histogram using ImageJ software and are shown in Figure 13b.

Conclusion

Herein, we report on the successful synthesis of GOQDs via the one-pot pyrolysis of citric acid. The synthesized GOQDs were characterized using microscopic and spectroscopic techniques. The XRD data shows that the GOQDs are structurally similar to graphite. The morphology of the GOQDs was found to be spherical, non-aggregated and of 4.3 nm in size. The GOQD photocatalysts were found to be more efficient in the detoxification and discoloration of the BB dye from the spiked real wastewater sample than that from the synthetic water sample. Additionally, an increase in the initial concentration of the BB dye negatively influenced the photocatalytic activity of GOQDs. It was shown that the synthetic water and spiked wastewater samples possessed higher reaction rates at lower BB concentrations, and when the concentrations increased, the reaction rates decreased. The results demonstrate that an increase in reaction rate constant resulted in faster dye discoloration, higher catalytic activity and reduced half-lives. The degradation mechanism is postulated to be a combination of both photocatalytic degradation and photosensitization of the dye, with the photocatalytic degradation being the more dominant mechanistic pathway. The reusability experiment shows that the degradation rates of the GOQDs decreased gradually from 98.0% of the first cycle to 85.9% after the fourth cycle. The reusability performances of the GOQDs indicate that GOQDs are stable and recyclable and can be tested in the real wastewater treatment plant. The upscaling of this study is envisaged to ensure that the use of GOQDs for efficient detoxification and discoloration of the harmful dye from a real wastewater treatment plant can be successfully applied. During the photodegradation process, the hydroxyl radicals (highly reactive and nonselective species) react with the complex organic and inorganic compounds to produce less complex and less harmful compounds. In a real wastewater treatment plant, this would minimize sludge formation, and such a system would result in a faster wastewater treatment process.

Acknowledgements We gratefully acknowledge the partial financial support from University of South Africa and the National Research Foundation of South Africa.

Funding This study was funded in part by the National Research Foundation of South Africa (grant numbers 129350)

Declarations

Conflict of interest The authors declare no competing interests.

References

Avisar D, Horovitz I, Lozzi L, Ruggieri F, Baker M, Abel ML, Mamane H (2013) Impact of water quality on removal of carbamazepine in natural waters by N-doped TiO_2 photo-catalytic thin film surfaces. J Hazard Mater 244:463–471

Chhabra VA, Kaur R, Kumar N, Deep A, Rajesh C, Kim KH (2018) Synthesis and spectroscopic studies of functionalized graphene quantum dots with diverse fluorescence characteristics. RSC Adv 8:11446–11454

Gandhi MR, Vasudevan S, Shibayama A, Yamada M (2016) Graphene and graphene-based composites: a rising star in water purification - a comprehensive overview. Chemistry Select 1:4358–4385

Ge J, Lan M, Liu W, Jia Q, Guo L, Zhou B, Meng X, Niu G, Wang P (2016) Graphene quantum dots as efficient, metal-free, visible -light-active photocatalysts. Sci China Mater 59(1):12–19

Hashemzadeh H, Hasanzadeh M, Shadjou N, Eivazi-Ziaei J, Khoubnasabjafari M, Jouyban A (2016) Graphene quantum dot modified glassy carbon electrode for the determination of doxorubicin hydrochloride in human plasma. J Pharm Anal 6:235–241

He Y, Sutton NB, Rijnaarts HHH, Langenhoff AAM (2016) Degradation of pharmaceuticals in wastewater using immobilized TiO_2 photocatalysis under simulated solar irradiation. Appl Catal B Environ 132–141.

Jalloulia N, Pastrana-Martínezb LM, Ribeirob AR, Moreirab FF, Fariab JL, Hentatia O, Silvab AMT, Ksibia M (2018) Heterogeneous photocatalytic degradation of ibuprofen in ultrapure water, municipal and pharmaceutical industry wastewaters using a TiO_2/UV-LED system. Chem Eng J 976–984.

Kim CO, Hwang SW, Kim S (2014) High-performance graphene-quantum-dot photodetectors. Sci Rep 4 5603-5621.

Konkena B, Vasudeva S (2012) Understanding aqueous dispersibility of graphene oxide and reduced graphene oxide through pKa measurements. J Phys Chem Lett 3:867–872

Kudin KN, Ozbas B, Schniepp HC, Prud'homme RK, Aksay IA, Car R (2008) Raman spectra of graphite oxide and functionalized graphene sheets. Nano Lett 8: 36-41.

Kumar P, Panchakarla LS, Bhat SV, Maitra U, Subrahmanyam KS, Rao CNR (2010) Photoluminescence, white light emitting properties and related aspects of ZnO nanoparticles admixed with graphene and GaN. Nanotechnology 21(38):385701–3857119

Lima CS, Batista KA, García Rodríguez A, Souza JR, Fernandes KF (2015) Photodecomposition and color removal of a real sample of textile wastewater using heterogeneous photocatalysis with polypyrrole. Sol Energy 105–113.

Loh KP, Bao Q, Eda G, Chhowalla M (2010) Graphene oxide as a chemically tunable platform for optical applications. Nat Chem 2:015–1024

Manna S, Bhattacharya S, Sengupta S, Das P (2018) Synthesis of graphene oxide dots coated biomatrices and its application for the removal of multiple pollutants present in wastewater. J Clean Prod 203:83–88

Matamoros V, Duhec A, Albaiges J, Bayona, (2008) Photodegradation of carbamazepine, ibuprofen, ketoprofen and 17α-ethinylestradiol in fresh and seawater. J Water Air Soil Prod 196(1):161–168

Muleja AA, Mamba BB (2018) Development of calcined catalytic membrane for potential photodegradation of Congo red in aqueous solution. J Environ Chem Eng 4:4850–4863

Pan DY, Zhang JC, Li Z, Wu MH (2010) Hydrothermal route for cutting graphene sheets into blue-luminescent graphene quantum dots. Adv Mater: 734–738.

Putri LK, Tan LL, Ong WJ, Chang WS, Chai SP (2016) Graphene oxide: exploiting its unique properties toward visible-light-driven photocatalysis. App Mater Today 4:9–16

Puvvada N, Kumar BNP, Konar S, Kalita H, Mandal M, Pathak A (2012) Synthesis of biocompatible multicolor luminescent carbon dots for bioimaging applications. Sci Technol Adv Mater 13:045008–045015

Qu D, Zheng M, Du P, Zhou Y, Zhang L, Li D, Sun Z (2013) Highly luminescent S, N co-doped graphene quantum dots with broad visible absorption bands for visible light photocatalysts. Nanoscale 5:12272–12277

Rahimi K, Yazdani A, Ahmadirad M (2018) Facile preparation of zinc oxide nanorods surrounded by graphene quantum dots both synthesized via separate pyrolysis procedures for photocatalyst application. Mater Res Bull 98:148–154

Rajabi HR, Farsi M (2015) Effect of transition metal ion doping on the photocatalytic activity of ZnS quantum dots: synthesis, characterization, and application for dye decolorization. J Mol Catal A Chem 399(2015):53–61

Roushani M, Mavaei M, Rajabi HR (2015) Graphene quantum dots as novel and green nano-materials for the visible-light-driven photocatalytic degradation of cationic dye. J Mol Catal a: Chem 409:102–109

Rueda-Marquez JJ, Levchuk I, Ibanez PF, Sillanpää M (2020) A critical review on application of photocatalysis for toxicity reduction of real wastewaters. J Clean Prod 258:120694–120707

Sapra S, Sarma DD (2005) Simultaneous control of nanocrystal size and nanocrystal-nanocrystal separation in CdS nanocrystal assembly. Pramana 65:565–570

Shafaee M, Goharshadi EK, Mashreghi M, Sadeghinia M (2018) TiO2 nanoparticles and TiO2@ graphene quantum dots nancomposites as effective visible/solar light photocatalysts. J Photochem Photobiol A 357:90–102

Shao M, Han J, Wei M, Evans DG, Duan X (2011) The synthesis of hierarchical Zn–Ti layered double hydroxide for efficient visible-light photocatalysis. Chem Eng J 168(2):519–524

Sharma NK, Philip L (2016) Combined biological and photocatalytic treatment of real coke oven wastewater. Chem Eng J 295:20–28

Shen J, Zhu Y, Yang X, Li C (2012) Graphene quantum dots: emergent nanolights for bioimaging, sensors, catalysis and photovoltaic devices. Chem Commun 48:3686–3699

Sobon G, Sotor J, Jagiello J, Kozinski R, Zdrojek M, Holdynski M, Paletko P, Boguslawski J, Lipinska L, Abramski KM (2012) Graphene oxide vs. reduced graphene oxide as saturable absorbers for Er-doped passively mode-locked fiber laser. Opt Express 20:19463–19473

Souza RP, Freitas TKFS, Domingues FS, Pezoti O, Ambrosio E, Ferrari-Lima AM, Garcia JC (2016) Photocatalytic

activity of TiO_2, ZnO and Nb_2O_5 applied to degradation of textile wastewater. J Photochem Photobiol Chem 9–17.

Štengl V, Bakardjieva S, Henych J, Lang K, Kormunda M (2013) Blue and green luminescence of reduced graphene oxide quantum dots. Carbon 63:537–546

Syam Babu D, Srivastava V, Nidheesh PV, Kumar M (2019) Detoxification of water and wastewater by advanced oxidation processes. Sci Total Environ 696:133961–133981

Talwara S, Sangala VK, Verma A (2018) Feasibility of using combined TiO_2 photocatalysis and RBC process for the treatment of real pharmaceutical wastewater. J Photo Photobio a: Chemistry 353:263–270

Tang L, Ji R, Cao X, Lin J, Jiang H, Li X, Teng KS, Luk CM, Zeng S, Hao J (2012) Deep ultraviolet photoluminescence of water-soluble self-passivated graphene quantum dots. ACS Nano 6:5102–5110

Tetsuka H, Asahi R, Nagoya A, Okamoto K, Tajima I, Ohta R, Okamoto A (2012) Optically tunable amino-functionalized graphene quantum dots. Adv Mater 24:5333–5338

Topkaya E, Konyar M, Yatmaz HC, Öztürk K (2014) Pure ZnO and composite ZnO/TiO_2 catalyst plates: a comparative study for the degradation of azo dye, pesticide and antibiotic in aqueous solutions. J Colloid Interface Sci 430:6–11

Tsai C-G, Tseng WJ (2020) Preparation of TiN–TiO_2 composite nanoparticles for organic dye adsorption and photocatalysis. Ceram Int 46:14529–14535

Tshangana C, Chabalala M, Muleja A, Nxumalo E, Mamba B (2020a) Shape-dependant photocatalytic and antimicrobial activity of ZnO nanostructures when conjugated to graphene quantum dots. J Environ Chem Eng 8:103930–103942

Tshangana CS, Muleja AA, Nxumalo EN, Mhlanga SD (2020) Poly (ether) sulfone electrospun nanofibrous membranes embedded with graphene oxide quantum dots with antimicrobial activity. Environ Sci Pollut Res. 26845–26855.

Vela N, Calín M, Yáñez-Gascón MJ, Garrido I, Pérez-Lucas G, Fenoll J, Navarro S (2018b) Photocatalytic oxidation of six endocrine disruptor chemicals in wastewater using ZnO at pilot plant scale under natural sunlight. Environ Sci Pollut Control Ser 35(25):34995–35007

Vela N, Calín M, Yáñez-Gascón MJ, Garrido I, Pérez-Lucas G, Fenoll J, Navarro S (2018) Photocatalytic oxidation of six pesticides listed as endocrine disruptor chemicals from wastewater using two different TiO_2 samples at pilot plant scale under sunlight irradiation. J Photochem Photobiol Chem 271–278.

Wang J, Guoa Y, Liu B, Xu B (2011) Detection and analysis of reactive oxygen species (ROS) generated by nano-sized TiO_2 powder under ultrasonic irradiation and application in sonocatalytic degradation of organic dyes. Ultrason Sonochem 18:177–183

Wang Y, Bi N, Zhang H, Tian W, Zhang T, Wu P, Jiang W (2020) Visible-light-driven photocatalysis-assisted adsorption of azo dyes using Ag_2O. Colloids Surf A Physicochem 585:1245–124120

Xiang X, Xie L, Li Z, Li F (2013) Ternary MgO/ZnO/In_2O_3 heterostructured photocatalysts derived from a layered precursor and visible-light-induced photocatalytic activity. Chem Eng J 221:222–229

Xiong J, Li X, Huang J, Gao X, Chen Z, Liu J, Li H, Kang B, Yao W, Zhu Y (2020) CN/rGO@BPQDs high-low junctions with stretching spatial charge separation ability for photocatalytic degradation and H_2O_2 production. Appl Catal B Environ. 266:118602–118621

Xu J, Huang J, Wang Z, Zhu Y (2020) Enhanced visible-light photocatalytic degradation and disinfection performance of oxidized nanoporous g-C_3N_4 via decoration with graphene oxide quantum dots. Chinese. J Catal 41: 474-484.

Zhang M, Bai L, Shang W, Xie W, Ma H, Fu Y, Fang D, Sun H, Fan L, Han M, Liu C, Yang S (2012) Facile synthesis of water-soluble, highly fluorescent graphene quantum dots as a robust biological label for stem cells. J Mater Chem 22:7461–7467

Zhang R, Liu Y, Yu L, Li Z, Sun S (2013) Preparation of high-quality biocompatible carbon dots by extraction, with new thoughts on the luminescence mechanisms. Nanotechnology 24:225601

Zhang S, Sui L, Dong H, He W, Dong L, Yu L (2018) High-performance supercapacitor of graphene quantum dots with uniform sizes. ACS Appl Mater Interfaces 10:12983–12991

Zhu S, Zhang J, Qiao C, Tang S, Li Y, Yuan W, Li B, Tian L, Liu F, Hu R (2011) Strongly green-photoluminescent graphene quantum dots for bioimaging applications. Chem Commun 47:6858–6860